INSTITUTE OF PHYSICS PUBLISHING JOURNAL OF MICROMECHANICS AND MICROENGINEERING
J. Micromech. Microeng. **15** (2005) 351–357 doi:10.1088/0960-1317/15/2/015

Comments on determining the elastic modulus of a thin film using the micromachined free–free beam

Chisheng Yu, Changchun Hsu and Weileun Fang

Department of Power Mechanical Engineering, National Tsing Hua University, Hsinchu, Taiwan

E-mail: fang@pme.nthu.edu.tw

Received 29 July 2004, in final form 14 October 2004
Published 24 November 2004
Online at stacks.iop.org/JMM/15/351

Abstract
The study investigates the vibration characteristics of the micromachined free–free beam through analytical and experimental means. In application, this study employed the resonant frequency of the micromachined free–free beam to successfully extract the elastic modulus of a thin film. As a comparison, the vibration characteristics of a micromachined cantilever have also been studied. This study demonstrates that the micromachined free–free beam is a better test key to extract the thin film elastic modulus when the wafer experiences a relatively long etching time. Moreover, the micromachined cantilever gives a lower bound and the micromachined free–free beam gives an upper bound while determining the thin film elastic modulus. Since the free–free beam is a previously fabricated and modeled micromachined structure, it can be employed as a supplement test key to the cantilever beam approach.

1. Introduction

The vibration characteristics of micromachined structures have been applied extensively in the MEMS area. For instance, the optical scanner [1], RF filter and resonator [2, 3] and bio-sensor [4] have all been studied. The resonant frequency of micromachined diagnostic structures (test key) has been exploited to determine the mechanical properties of thin films [5–8]. There are various advantages of using the resonant approach to measure the thin film material properties: (1) the available test structure is easily fabricated and modeled, (2) no physical contact with the test structure is required during the experiment and (3) the dynamic response at resonant frequency is large and sensitive.

Presently, the most popular test structures for thin film characterization are micromachined bridges [5] and cantilevers [6–8]. The resonant frequency of a micromachined cantilever has been extensively employed to determine the elastic modulus and Poisson's ratio of thin films [6–8]. However, the boundary condition of a bulk micromachined cantilever is influenced by the undercut of the substrate during bulk silicon etching. Moreover, the surface micromachined cantilever is not clamped perfectly due to the existence of a step at its boundary. In this regard, the boundary of a micromachined cantilever should be modeled as the combination of a linear and a torsional spring. With increased etching time, the undercut effect is even more severe. Thus, the thin film elastic modulus determined from the micromachined cantilever test key is significantly influenced by the fabrication processes. The boundary conditions of a micro bridge on a (100) single crystal silicon substrate are also very complicated [9]. In addition, the micro bridge test key has no free end to release the thin film residual stresses. The micro bridge will be tensed by residual tension and buckled by residual compression. Thus, it is difficult to accurately model the structural dynamics of the micro bridge.

This study investigates the vibration characteristics of a micromachined free–free beam through analytical and experimental means. In application, this study has successfully employed the micromachined free–free beam to extract the elastic modulus of a thin film. As a comparison, the thin film elastic modulus extracted from the micromachined cantilever test key is also provided. This work reduces the uncertainty of boundary conditions for different micromachined test structures during a vibration test.

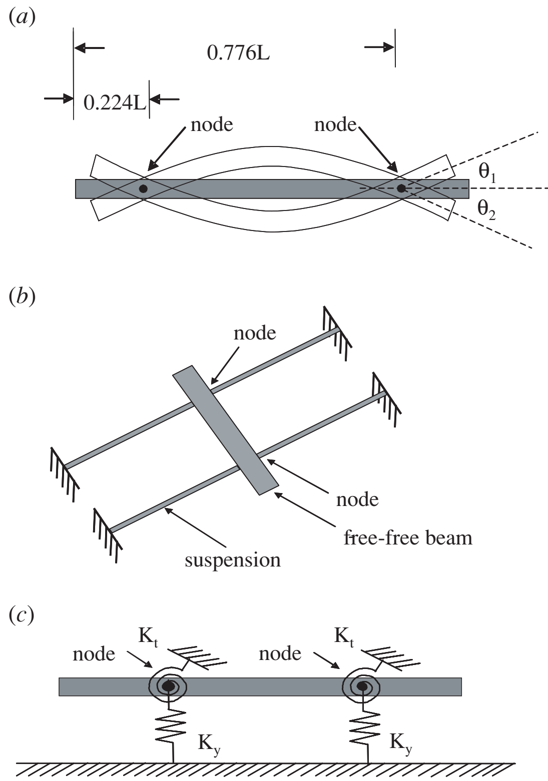

Figure 1. Schematic illustrations of (*a*) the ideal first flexure mode of the free–free beam, (*b*) the micromachined free–free beam and (*c*) the physical model of the micromachined free–free beam.

2. Designs and analysis

The first flexural bending mode of a free–free beam, as shown in figure 1, has been employed to determine the elastic modulus of bulk materials. The test standard of this free–free beam technique is properly defined by the American Society for Testing Materials (ASTM) [10]. The thin film elastic modulus can also be extracted from the resonant frequency f_n (for flexure bending modes) of a micromachined free–free beam. Based on the Euler–Bernoulli beam model, the elastic modulus E can be expressed as [11]

$$E = \frac{48\pi^2 \rho L^4 (f_n)^2}{(\beta_n L)^4 h^2} \tag{1}$$

where ρ, L and h are the density, length and thickness of the free–free beam, respectively. In addition, the parameter $\beta_n L$ is a constant associated with the nth flexure modes of the free–free beam and $\beta_1 L = 4.73$.

To survive after the micromachining processes, the micromachined beams have to be connected (or anchored) to the substrate. This study employed four springs to support the free–free beam, as shown in figure 1(*b*). Additionally, these four springs were designed to reduce the influence of the vibration characteristics of the free–free beam. In this regard, these four springs were connected to the nodes of the first flexure mode of the free–free beam, as indicated in figure 1(*b*). Figure 1(*c*) shows the physical model of the micromachined free–free beam. Hence, the bending deflection of the suspension due to the first flexure mode of the free–free beam was significantly reduced. However, as indicated in figure 1(*a*), the angular deflection of the nodes (from θ_1 to θ_2) cannot be ignored. This will lead to the twisting of these four springs. Thus, an ideal micromachined free–free beam can be realized if the torsional stiffness of these four springs is very small. In this study, commercial finite element method (FEM) software was employed to determine the variation of the spring stiffness with the natural frequency of the beam.

In addition to the FEM, the analytical solution of the first bending resonant frequency of the micromachined free–free beam shown in figure 1(*c*) was also established. Rayleigh's method was applied to find an approximation for the first natural frequency f_1 of the free–free beam. When vibrating at the first flexural mode, the maximum kinetic energy of the free–free beam in figure 1(*c*) can be expressed as [12]

$$T_{\max} = \frac{(2\pi f_1)^2}{2} \int_0^L \rho A[\Psi(x)]^2 \, dx. \tag{2}$$

In equation (2), $\Psi(x)$ is the shape function for the first natural frequency f_1 of the free–free beam, and can be represented as [12]

$$\Psi(x) = C_n[\sin \beta_1 x + \sinh \beta_1 x + \alpha_1(\cos \beta_1 x + \cosh \beta_1 x)] \tag{3}$$

where C_n is a constant, and the parameter α_1 is expressed as

$$\alpha_1 = \frac{\sin \beta_1 L - \sinh \beta_1 L}{\cosh \beta_1 L - \cos \beta_1 L}$$

and the parameter $\beta_1 L = 4.73$. Moreover, the maximum potential energy of the free–free beam for the first flexural mode becomes

$$V_{\max} = \frac{1}{2}\int_0^L EI\left[\frac{d^2\Psi(x)}{dx^2}\right]^2 dx + \frac{1}{2}K_t\left[\frac{d\Psi(x)}{dx}\right]^2\Bigg|_{\substack{x=0.224L\\x=0.776L}} + \frac{1}{2}K_y[\Psi(x)]^2\Bigg|_{\substack{x=0.224L\\x=0.776L}} \tag{4}$$

where $x = 0.224L$ and $x = 0.776L$ are the location of the two nodes. Two more potential energy terms are contributed by the twisting deformation of the torsional spring K_t and the transverse deflection of the linear spring K_y. The total energy is constant for a conservative system; in other words, $T_{\max} = V_{\max}$. According to equations (2) and (4), the first natural frequency of the free–free beam is determined from Rayleigh's quotient,

$$(f_1)^2 = \frac{\int_0^L EI\left[\frac{d^2\Psi(x)}{dx^2}\right]^2 dx + \frac{1}{2}K_t\left[\frac{d\Psi(x)}{dx}\right]^2\Big|_{\substack{x=0.224L\\x=0.776L}} + \frac{1}{2}K_y[\Psi(x)]^2\Big|_{\substack{x=0.224L\\x=0.776L}}}{4\pi^2\int_0^L \rho A[\Psi(x)]^2 \, dx}. \tag{5}$$

Therefore, the thin film elastic modulus E can be determined from equation (5) after the resonant frequency f_1 (the first flexural mode) of a micromachined free–free beam is measured.

The torsional stiffness of the suspensions can be tuned by varying their length and width. However, the minimum beam width is limited to the fabrication processes such as photolithography and etching. Figure 2 shows typical simulation and analytical results of the variation of the first bending resonant frequency with the suspension length, and the suspension width is specified as 5 μm. In this case, the

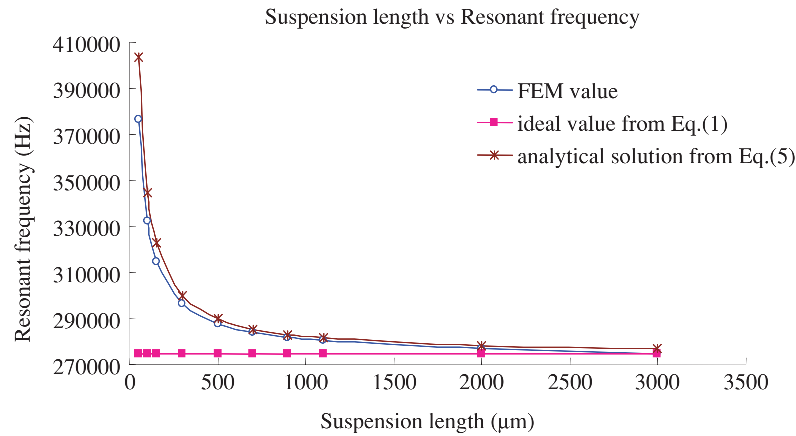

Figure 2. Variation of the resonant frequency with the suspension length from simulation and analysis.

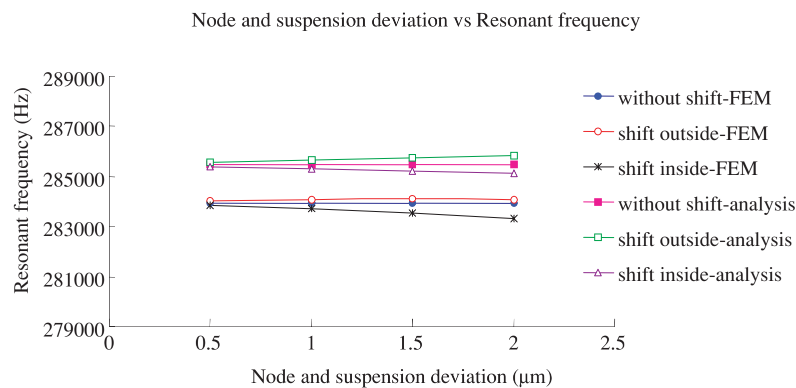

Figure 3. Variation of the predicted resonant frequency of the free–free beam due to the misalignment of the suspension and node.

deviation of resonant frequency between the ideal and the micromachined free–free beam is less than 4% when the spring length is more than 600 μm. Also, when the suspension length increases from 100 μm to 500 μm, the deviation between FEM and analytical solutions decreases from 3.8% to 0.7%. Therefore, the analytical solutions agree well with the FEM simulation results.

The suspensions may not precisely connect to the nodes after the fabrication processes. Hence, the influence of the misalignment between the nodes and the suspensions has also been studied by the FEM simulation. Figure 3 shows the variation of frequency shift due to the misalignment of the node and the suspension. The solid circles indicate the simulated resonant frequency of the micromachined free–free beam when the suspensions are aligned perfectly with the nodes. The open circles are the simulated resonant frequency of the free–free beam when the suspensions are shifted to the edge (outside) of the beam. The cross dots show the simulated resonant frequency of the micromachined free–free beam when the suspensions are shifted toward the middle (inside) of the beam. The analytical results available in figure 3 show the same tendency. In short, the frequency shifts are all less than 0.25% for a 2 μm deviation of the suspensions. Moreover, the free–free beam could be bent by the gradient residual stress of the thin film. The simulation results show that the resonant frequency shift is less than 1.8% even though the beam is bent with the radius of curvature of 1 mm.

3. Experiments

The bulk micromachined SiO_2 free–free beam was employed as the specimen for experimentation. During the vibration test, the SiO_2 free–free beams were excited by the PZT transducer and the dynamics of these test structures were characterized using the laser Doppler vibrometer (LDV).

3.1. Specimen preparation

In this experiment the SiO_2 free–free microbeams, with the length ranging from 250 μm to 500 μm, were fabricated through bulk micromachining. Three different beam widths (5 μm, 10 μm and 15 μm) were available for tests. The torsional spring was 5 μm wide, and its length ranged from 50 μm to 1100 μm. The (100) single crystal silicon substrate was placed in the furnace to grow 0.85 μm and 2 μm thick thermal oxide films at 1050 °C. The thermal oxide was patterned using reactive ion etching (RIE) after the photolithography. After the substrate was etched anisotropically by tetra-methyl ammonium hydroxide (TMAH), the micromachined beams and torsional springs were fully suspended. The process flow is shown in figure 4. The scanning electronic microscope (SEM) photo in figure 5 shows a typical micromachined free–free beam. This micromachined free–free beam was aligned 45° to the major flat edge of the (100) silicon substrate, so as to significantly reduce the bulk etching time.

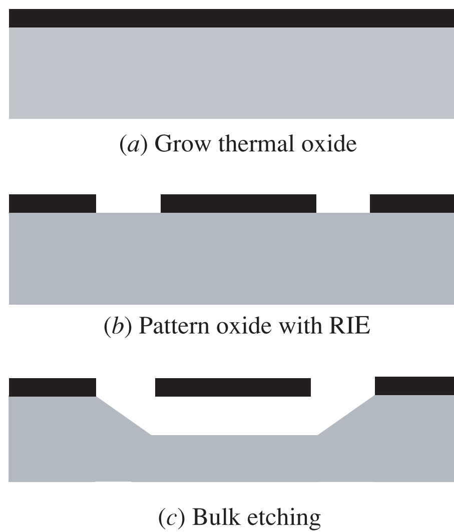

Figure 4. Fabrication process flow.

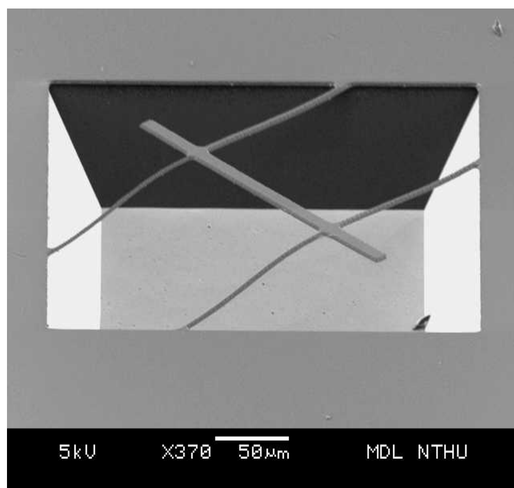

Figure 5. The SEM photo of a typical micromachined free–free beam.

3.2. Experiment setup

The experiment setup is shown in figure 6. The PZT transducer was employed to excite the micromachined beams. The function generator and power amplifier in figure 6 were used to produce a harmonic signal to drive the ultrasonic PZT transducer. The function generator together with the power amplifier can also be replaced by a pulse generator system. Finally, the dynamic response of the microstructures was measured from the LDV system. Both the time and frequency responses of the microstructures can be recorded and analyzed in the oscilloscope or frequency analyzer. The vacuum chamber was also available in the experiment to prevent the air effect (for example, spring, mass or damping) during the vibration test.

3.3. Experimental results

Figure 7 shows the typical measurement results of the suspension length versus resonant frequency. In this experiment, the test free–free beam was 2 μm thick, 15 μm wide and 250 μm long, with the suspension length ranging from 50 μm to 500 μm. The resonant frequency of the micromachined free–free beam gradually converges to a value as the suspension length increases. The measurement results show good agreement with the simulation shown in figure 2.

The resonant frequency shift that resulted from the misalignment of the suspension and the node was also characterized. The measurement results are shown in figure 8. The results indicate that the resonant frequency shift of the micromachined free–free beam is less than 2.4% even if the misalignment of the node and the suspension reaches ± 8.5 μm. Thus, the misalignment of the node and the suspension due to the fabrication processes has very little influence on the resonant frequency and mode shape. Therefore, this effect can be ignored.

4. Applications and discussions

In application, this study extracted the elastic modulus of SiO_2 thin film from equation (1) after the resonant frequency of the micromachined free–free test beam was determined. As shown in figure 7, the resonant frequency of the free–free beam will converge to the ideal value as the suspension length increases. The elastic modulus of the thin film will also converge from a larger value. In other words, the elastic

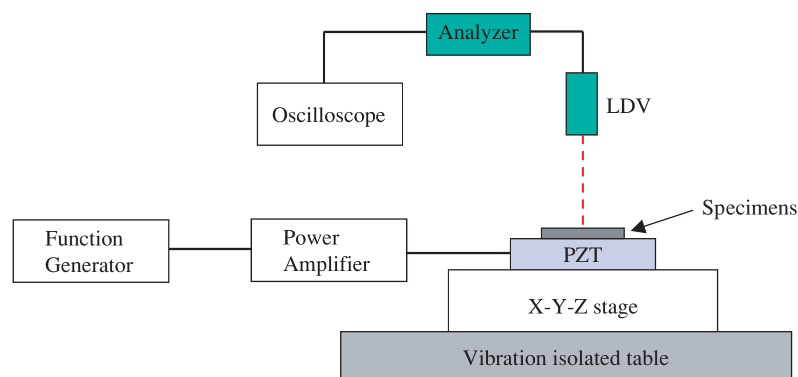

Figure 6. Measurement equipment setup.

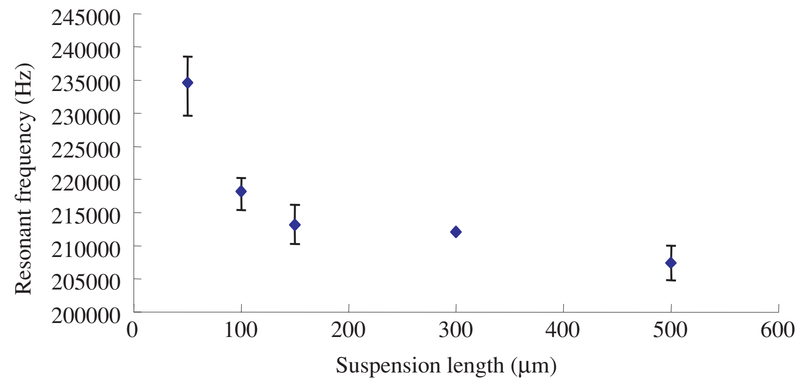

Figure 7. Variation of the measured resonant frequency with the suspension length.

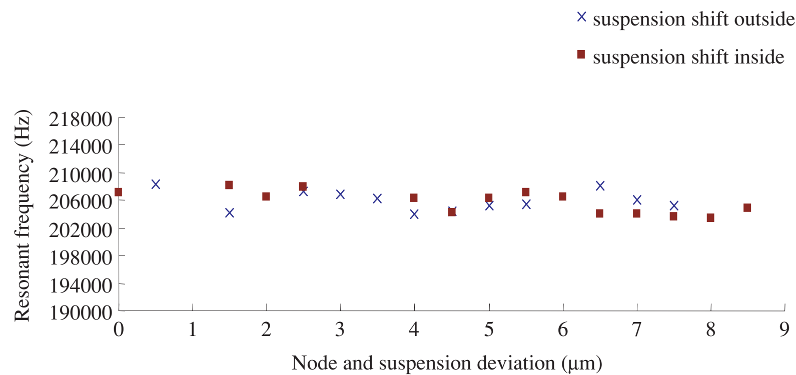

Figure 8. Variation of the measured resonant frequency of the free–free beam due to the misalignment of the suspension and node.

modulus determined using the aforementioned free–free beam approach provides an upper bound of the exact value. The elastic modulus of the SiO_2 film measured using this approach converged to 75.6 GPa when the suspension was increased to 500 μm. As the suspension increased to 900 μm, the elastic modulus of the SiO_2 film further converged to 67.9 GPa. In comparison, the elastic modulus of the SiO_2 film extracted from the micromachined cantilever test key was 67.2 GPa.

The resonant frequency of a micromachined cantilever has also been extensively employed to determine the elastic modulus of thin films [6–8]. It is well known that the boundary of a surface micromachined cantilever is not clamped perfectly due to the step-up at its anchor. The boundary condition of a bulk micromachined cantilever is influenced by the undercut, and varies with the etching time. The boundary of an ideal bulk micromachined cantilever will be precisely defined by {111} planes after anisotropic etching of a {100} oriented silicon wafer. In reality, the selectivity for {100} planes over {111} planes is not infinite during anisotropic etching. The {111} planes are gradually attacked, so that the boundary of the cantilever will be undercut as shown in figure 9(*a*). In this regard, the no-slope and no-displacement boundary conditions for the ideal cantilever are no longer valid. The boundary should be modeled as a combination of a linear (K_y) and a torsional (K_t) spring as shown in figure 9(*b*). Thus, the resonant frequency of the micromachined cantilever is smaller than the ideal case. The elastic modulus determined from the resonant frequency will also be smaller than the exact value. Moreover, with the increment of the etching time, the undercut effect is even more severe. Thus, the thin film elastic modulus determined using the resonant frequency of

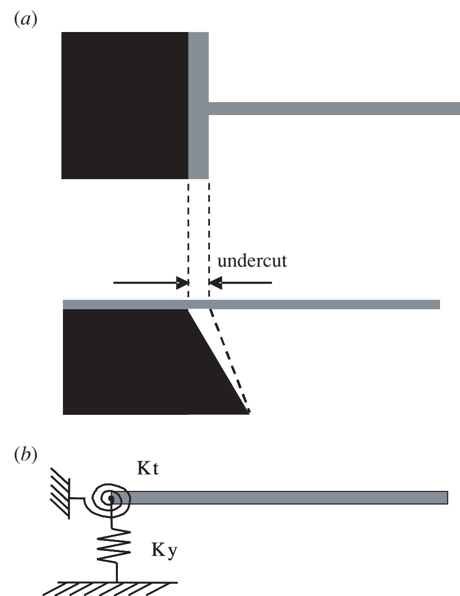

Figure 9. The boundary undercut of cantilever (*a*) top and side views and (*b*) physical model.

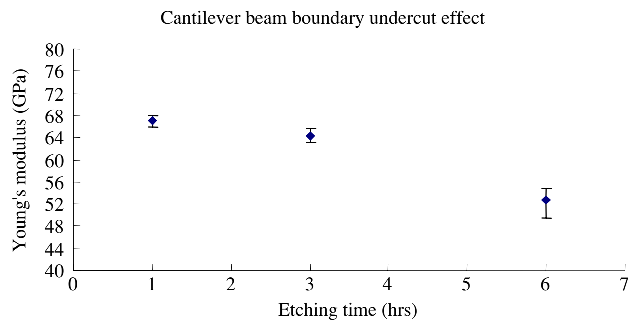

Figure 10. The elastic modulus determined from the micromachined cantilever test key at three different bulk etching time points.

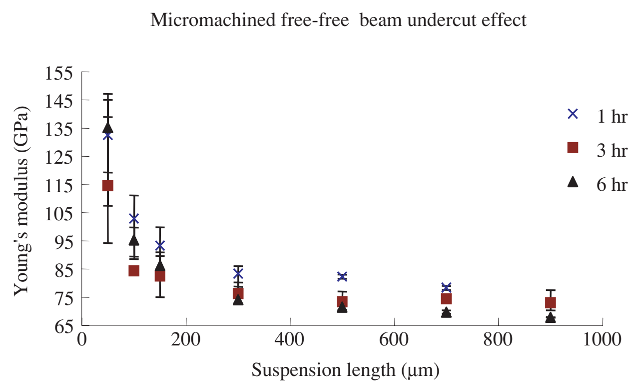

Figure 11. Variation of the elastic modulus determined from the micromachined free–free beam test key with the suspension length at three different bulk etching time points.

the micromachined cantilever is significantly influenced by the fabrication processes.

Figure 10 shows the variation of the elastic modulus determined using the micromachined cantilever test key at three different etching time points. The experimental results showed that the elastic modulus of SiO_2 film determined after 1 h bulk etching was 67.2 GPa. After bulk etching for 6 h, the undercut effect led to a significant drop of natural frequency of cantilevers. Although the variation of film thickness during etching was considered, the elastic modulus of SiO_2 film extracted from the natural frequency of the micromachined cantilever was still reduced to 52.7 GPa. In short, the elastic modulus extracted from the micromachined cantilever test key dropped 21.5% after 6 h of etching time. Therefore, cantilevers are not an appropriate test key for longer etching times.

As for the micormachined free–free beam, the {111} planes are also attacked during bulk silicon etching. The undercut effect occurs at the boundary of suspensions, so as to reduce the stiffness of the torsional spring K_t in figure 1(*c*). Hence, the resonant frequency of the micromachined free–free beam is closer to that of the ideal one under the assistance of boundary undercut. In summary, the frequency of the micromachined free–free beam will approach the ideal value with a longer etching time. As shown in figure 11, the elastic modulus is determined using the micromachined free–free beam test key. Figure 11 shows the variation of the elastic modulus with the suspension length ranging from 50 μm to 900 μm at three different etching time points (1, 3 and 6 h). According to the measurement results, the torsional stiffness K_t of the suspension and the measured elastic modulus decreased with increased etching time. For instance, the measured elastic modulus of a 700 μm long suspension dropped from 78.3 GPa to 69.6 GPa when the etching time increased from 1 h to 6 h. In general, a more accurate elastic modulus can be extracted from the ideal free–free beam model for a longer etching time. Therefore, a micromachined free–free beam is a better test key for a longer etching time.

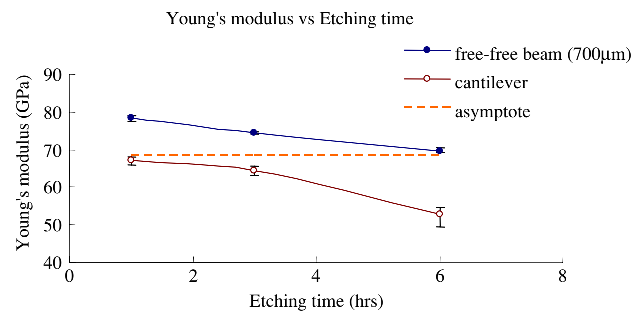

Figure 12. Elastic modulus extracted by the micromachined free–free beam and cantilever at different bulk etching time points.

In short, figure 12 shows variation of the measured elastic modulus with the etching time for both micromachined free–free beam and cantilever. According to the resonant beam technique, the cantilever test key provides a lower bound and the free–free beam test key provides an upper bound for the measured elastic modulus. A more accurate elastic modulus is obtained using the micromachined free–free beam test key for a longer etching time. On the other hand, a more accurate elastic modulus is obtained using the micromachined cantilever test key for a shorter etching time. The SiO_2 film elastic modulus determined using the micromachined free–free beam approach is 69.6 GPa (when the etching time is 6 h). As a comparison, the SiO_2 film elastic modulus extracted from the micromachined cantilever test key is 67.2 GPa (when the etching time is 1 h). Since the free–free beam is a readily fabricated and modeled micromachined structure, it can be employed as a supplement test key to the cantilever beam approach.

5. Conclusions

The vibration characteristics of the micromachined free–free beam have been discussed in this study. The resonant frequency and mode shape of the micromachined free–free beam influenced by suspensions and process are investigated through simulations and experiments. In application, this study employed the resonant frequency of the micromachined free–free beam to successfully extract the mechanical properties of SiO_2 thin film. As a comparison, the vibration characteristics of a micromachined cantilever have also been studied. However, the boundary condition of a bulk micromachined cantilever is influenced by the undercut, and varies with the etching time.

In conclusion, this study demonstrates that the micromachined free–free beam is a better test key to extract the thin film elastic modulus when the wafer experiences a

relatively long etching time. Moreover, the micromachined cantilever gives a lower bound and the micromachined free–free beam gives an upper bound for determining the thin film elastic modulus. Since the free–free beam is a readily fabricated and modeled micromachined structure, it can be employed as a supplement test key to the cantilever beam approach.

Acknowledgments

This research is based on the work supported by National Science Council of Taiwan under grant NSC-92-2212-E-007-052. The authors would like to thank the Central Regional MEMS Research Center of National Science Council, Semiconductor Research Center of National Chiao Tung University and National Nano Device Laboratory of NSC for providing the fabrication facilities.

References

[1] Wu M, Lai C-F and Fang W 2004 Integration of the DRIE, MUMPs, and bulk micromachining for superior micro-optical systems *IEEE MEMS'04 (Maastricht, The Netherlands, Jan. 2004)* pp 97–100

[2] Piekarski B, DeVoe D, Dubey M, Kaul R and Conrad J 2001 Surface micromachined piezoelectric resonant beam filters *Sensors Actuators* A **91** 313–20

[3] Wang K, Yu Y, Wong A-C and Nguyen C T-C 1999 VHF free–free beam high-Q micromechanical resonators *IEEE MEMS'99 (Orlando, FL, Jan. 1999)* pp 453–8

[4] Su M, Li S and Dravid V P 2003 Microcantilever resonance-based DNA detection with nanoparticle probes *Appl. Phys. Lett.* **82** 3562–4

[5] Zhang L M, Uttamchandani D, Culshaw B and Dobson P 1990 Measurement of Young's modulus and internal stress in silicon microresonators using a resonant frequency technique *Meas. Sci. Technol.* **1** 1343–6

[6] Petersen K E and Guarnieri C R 1979 Young's modulus measurements of thin films using micromechanics *J. Appl. Phys.* **50** 6761–6

[7] Tsai H-C and Fang W 2003 Determining the Poisson's ratio of thin film materials using resonant method *Sensors Actuators* A **103** 377–83

[8] Kiesewetter L, Zhang J-M, Houdeau D and Steckenborn A 1992 Determination of Young's moduli of micromechanical thin films using the resonance method *Sensors Actuators* A **35** 153–9

[9] Hu H-H, Lin H-Y, Fang W and Chou B C S 2001 The diagnostic micromachined beams on (111) substrate *Sensors Actuators* A **93** 258–65

[10] ASTM standard, C623-92 2000 Standard test method for Young's modulus, shear modulus, and Poisson's ratio for glass and glass-ceramics by resonance, ASTM International, West Conshohocken, PA

[11] Rao S S 1995 *Mechanical Vibrations* 3rd edn (Menlo Park, CA: Addison-Wesley)

[12] Meirovitch L 1967 *Analytical Methods in Vibrations* (New York: Macmillan)